





Hydrodynamic attraction of bacteria to gas and liquid interfaces

Adib Ahmadzadegan ¹, Shiyan Wang ², Pavlos P. Vlachos ¹, and Arezoo M. Ardekani ^{1,*}

¹*School of Mechanical Engineering, Purdue University, West Lafayette, Indiana 47907, USA*

²*Davidson School of Chemical Engineering, Purdue University, West Lafayette, Indiana 47907, USA*



(Received 26 February 2019; published 20 December 2019)

Near an interface, the distribution of swimming microorganisms such as bacteria is distinguished from inert colloidal particles because of the interfacial hydrodynamics induced by swimming. In this work, we use nontumbling flagellated bacteria, *Escherichia coli*, to study cell distribution near gas and liquid interfaces and compare it to the case of a solid wall. For low-viscosity ratios such as gas interfaces, we observe a stronger cell accumulation compared to that near liquid and solid surfaces. This contradicts known theoretical predictions. Therefore, we develop a model based on Brownian dynamics, including hydrodynamic effects and short-range physiochemical interactions between bacteria and interfaces. This model explains our experimental findings and can predict cell distribution near clean and surfactant-contaminated interfaces. By considering higher order singularities, this study helps explain bacteria orientation, trajectories, and cell density.

DOI: [10.1103/PhysRevE.100.062605](https://doi.org/10.1103/PhysRevE.100.062605)

I. INTRODUCTION

Understanding the interactions of active matters with their surrounding environment is of growing interest due to their prevalence in environmental remediation, biomedical devices [1], colloidal machines [2], and biological reproductions [3]. Many microorganisms, for example, marine bacteria, live in a liquid medium confined by various boundaries ranging from solids at the seafloor, to plant or coral surfaces, to liquid and gas interfaces, e.g., sea surface microlayer [4]. Previous studies have shown accumulation of microswimmers near solid surfaces. These cell accumulations have been experimentally observed for several bacteria strains [5–7], as well as animal and human spermatozoa [8]. Marine bacteria aggregations near oil-water interfaces were observed in the Deep Water Horizon oil spill [9]. Cell accumulations have also occurred near gas interfaces in microbiological systems such as biofilm formation at free surfaces (air-liquid interfaces) [10–12].

Hydrodynamics of liquid interfaces play a key role in pattern formation by self-assembly, colloidal binding by interparticle interactions, and recently, bacteria entrapment due to confinements [13–15]. Swimming microorganisms create flows that influence their interactions, nutrient uptake, and motility. In addition to hydrodynamic interactions between bacteria and boundary surfaces, microorganisms exhibit complex patterns because of Brownian motion [16]. Additionally, interfaces are the favorable location for the accumulation of bacteria-generated surfactants [17], which further complicates the analysis of bacteria swimming near interfaces. In this work, we examine the role of hydrodynamic interactions on bacteria suspensions near surfactant-contaminated interfaces.

To explain the cell accumulation near solid surfaces, several microbiological studies have measured the cell distribution as a function of the distance away from the surfaces [6–8]. Despite the high prevalence of bacteria interactions

with liquid and gas interfaces in real systems, bacteria accumulation near such interfaces remains less explored [15]. Here, we investigate the cell distribution near gas and liquid interfaces. We report a higher cell accumulation near a CO₂ interface compared to that near liquid and solid surfaces. A model using long-range hydrodynamics has been used in the past to predict the accumulation of bacteria near a wall [5]. Such a model, however, does not describe our experimental results near gas and liquid interfaces. Therefore, we develop a model including hydrodynamics and considering interfacial viscosity. In addition to using flow stresslet (force dipole) for hydrodynamic modeling, we include higher order flow singularities to explain the experimentally observed bacteria body axis tilting (“nose down”) near an interface and a wall [15,18].

II. EXPERIMENTS

A. Bacteria preparation

Nonchemotactic, nontumbling, motile *Escherichia coli* (HCB-437) is first grown on Luria broth agar plates overnight at 37 °C and single colonies are acquired. Selected colony is then cultured in Luria broth at 37 °C with a 150 RPM shaking rate and stopped at an optical density (OD) of ~1. A secondary culture from 1:100 dilution of the culture in a liquid Tryptone medium (1%TB, 0.5% sodium chloride) is made. The secondary culture is grown at 34 °C with a shaking rate of 200 rpm. To achieve the highest bacteria motility, the cell incubation is stopped at the mid-exponential phase (OD ~0.6). The cells are washed three times (2200 g for 8 min) and resuspended in motility medium (10⁻² M potassium phosphate, pH 7.0, 10⁻⁴ M EDTA) [5]. The washed cell suspension is then mixed with Percoll (2:3 ratio) to attain a density-matched solution [5].

B. Experimental procedure

We studied the distribution of *E. coli* cells near various fluid-fluid interfaces. To achieve a flat interface, we designed

*ardekani@purdue.edu

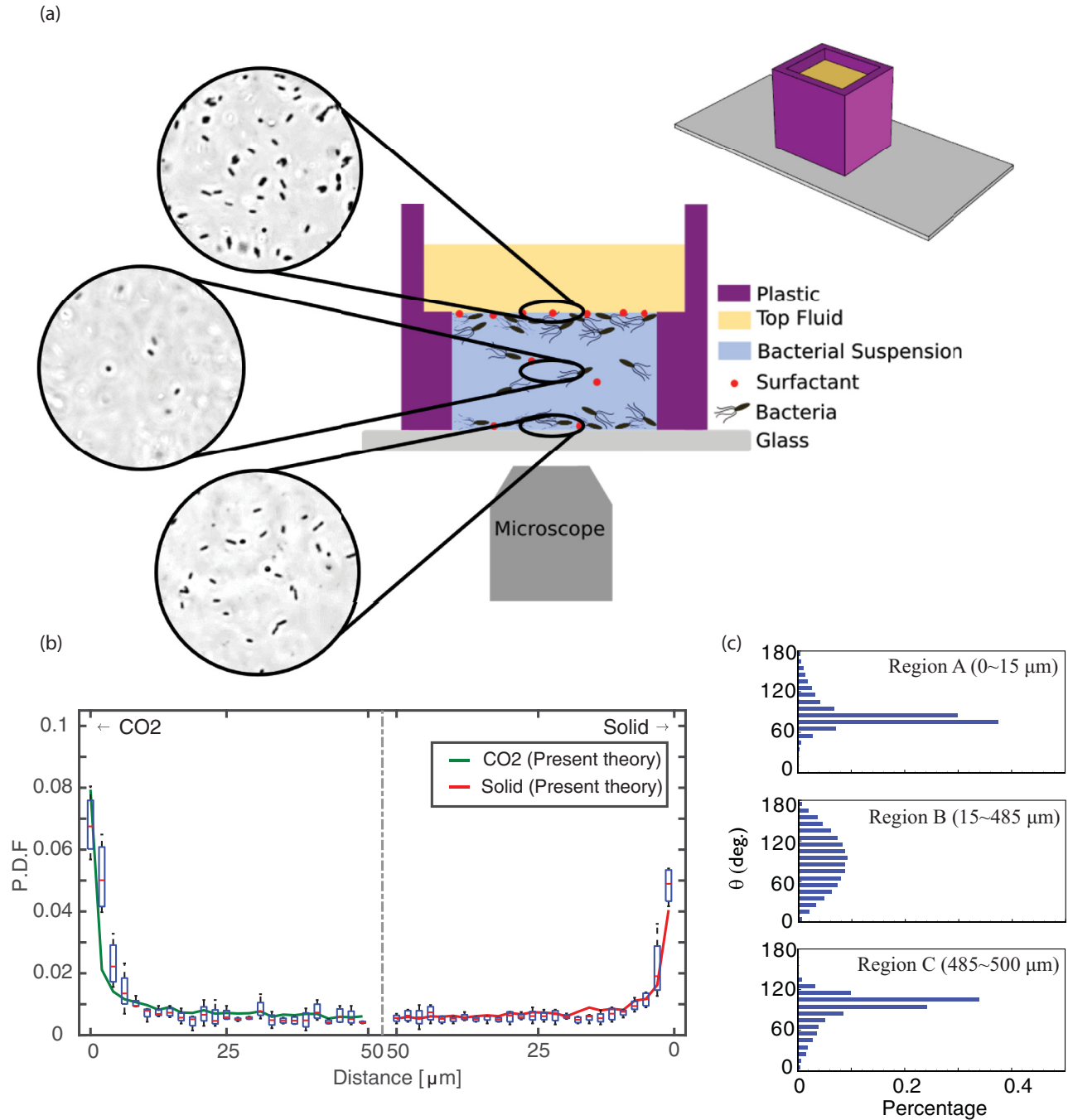


FIG. 1. (a) Experimental apparatus with showcase of cell counts (CO_2) in regions A, B, and C as defined in Fig. 4(a). (b) The comparison of probability density function between experimental (box plots) and numerical results (solid lines) for CO_2 ($\alpha = 34 \mu m^3 s^{-1}$, $\eta = 2.8 \mu m^4 s^{-1}$, $\tau = 58 \mu m^4 s^{-1}$, $\gamma = 7.5 \mu m^4 s^{-1}$) with surface viscosity $\beta = 1$ and channel depth $H = 500 \mu m$. (c) The spatial distribution of bacteria orientation is described as a histogram obtained from simulations.

a chamber with a small cross-sectional area with height of $H = 500 \mu m$ for the bacteria suspension at the bottom and a larger area for the top fluid [see Fig. 1(a)]. This microscopy setup was made by adhering a three-dimensional printed cubic wall on a microscopy glass coverslip. We filled this chamber with 0.3 ml of the density-matched cell solution and then added the second liquid with a known viscosity to the top. Note that the strong interfacial tension prevents bacteria from swimming into the top phase. In order to vary the viscosity

ratio λ , we considered dodecane, mineral oil, and soybean oil as top fluids. In addition, we examined two limits in terms of λ by considering a CO_2 interface and a solid surface (see Table I).

We placed the microscopy chamber on a piezo motorized stage of a Nikon Ti-e microscope. We utilized a $20\times$ objective lens and a phase contrast illumination technique to scan the chamber. A 5.5 Megapixel Zyla camera captured an imaging area of $256 \times 256 \mu m^2$. The scanning volume enclosed two

TABLE I. Viscosity ratios of two fluids in contact at room temperature.

Top phase	CO ₂	Dodecane	Mineral oil	Soybean oil	Solid
λ	0.016	1.3	24	50	∞

regions of 50 μm along the vertical direction starting from the top and bottom surfaces into the bacteria solution. Ten images were captured for every 2 μm at a frame rate of 10 frames per second.

We processed the images to first remove the mean vibration of the system using a cross-correlation-based image registration. Next, we tracked each individual bacterium from one frame to the next using a multiparametric object-tracking code. Size, intensity, and neighborhood distance are the matching parameters, to which we assigned equal weights in our analysis [19,20]. We considered the cells that swim a distance greater than one body length per second as motile. We calculate the number of motile cells at each level as the median value of motile cell counts of the 10 frames.

We performed four independent experiments for each viscosity ratio λ (Table I). Figure 1(b) shows a box plot of the probability density function (PDF) of cell counts near the CO₂ interface ($\lambda = 0.016$). Surprisingly, for the gas interface (i.e., CO₂), we observed higher accumulation near the interface than that from the wall [see Fig. 1(b)]. For higher viscosity ratios, the difference in accumulation is within the measured error bars of the experiments. For box plots of all λ cases see the Supplemental Material (see Fig. S1 in Ref. [21]). We found the median value of the four independent experiments and used them for further analysis [Figs. 2 and 5(a) below].

In the following sections, we propose a theoretical model to study the accumulation near gas and liquid interfaces and compare the simulation results with our experiments.

III. THEORETICAL MODELING

Multiple theoretical models have been proposed to predict cell attraction to solid surfaces. Li and Tang proposed that collisions with a surface and rotational Brownian diffusion are the primary reasons for the increased number of cells near a solid surface [22]. Berke *et al.* first explained the cell distributions near a solid surface using long-range microhydrodynamics [5,23]. This theory suggests that the number of cells n satisfies $n/n_o = \exp[L_p/Z]$, where Z is the distance measured from the interface, n_o represents cell number in the bulk, and L_p is the hydrodynamic length scale. This theoretical model is derived by balancing the convection driven by cell self-propulsion with cell diffusion near the wall. Near a clean interface, cell distributions can be similarly predicted as $n/n_o = \exp[(2 + 3\lambda)/(3 + 3\lambda)L_p/Z]$ [23]. Figure 2 presents the scaled cell number based on n_o and L_p where L_p is determined by fitting the median value of the four independent experiments for each viscosity ratio. This model, which considers only the effects of steady-state orientation and diffusion, underpredicts the scaled cell counts in our experiments.

Several studies have also focused on swimmer dynamics near clean or surfactant-contaminated interfaces [24]. Organic

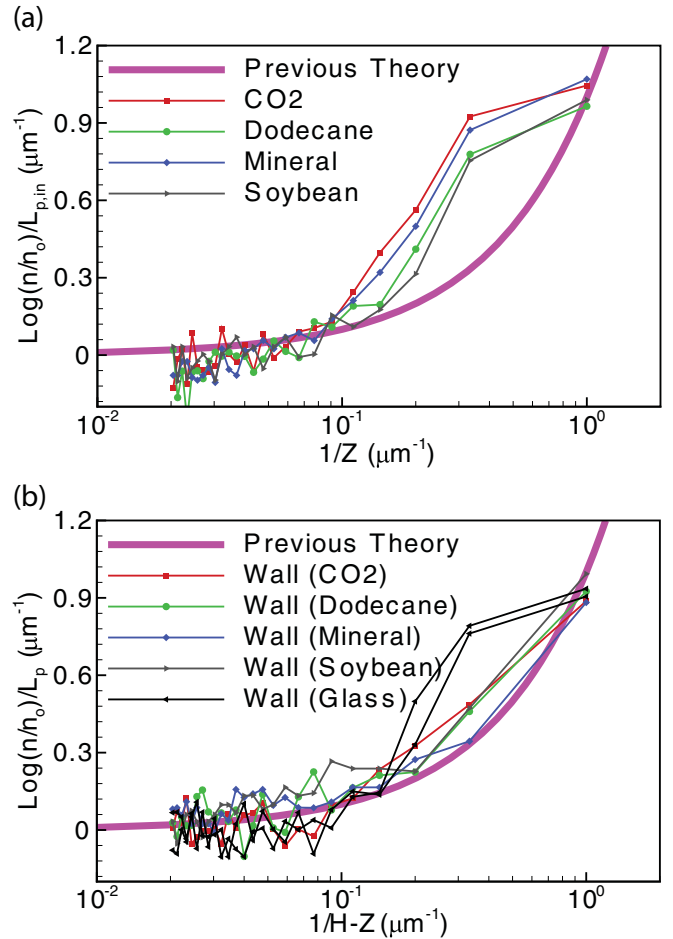


FIG. 2. Scaling by the previous model near (a) gas and liquid interfaces and (b) wall. $L_{p,\text{in}} = \frac{2+3\lambda}{3+3\lambda}L_p$, and L_p is a fitting parameter that varies for each viscosity ratio.

molecules from the growth medium get attached at the air-water interface, creating a highly viscous film such that the interface no longer acts as a free surface and creates hydrodynamic traps for bacteria [25]. Based on the previous theory [5] which considers the boundary effect, it has been shown that an interface with a partial slip boundary such as a surface covered with surfactant reorients the bacteria to the parallel direction, and the hydrodynamic attraction toward such interfaces is equivalent to the solid wall [23]. This theory, however, does not explain our results for bacteria distribution near liquid and gas interfaces.

Here, we present a numerical framework to model bacteria accumulation near liquid interfaces considering rotational Brownian motion, microhydrodynamics, physiochemical interactions (e.g., van der Waals, electrostatic, and excluded volume), and effects of interfacial viscosity. Our model quantitatively reproduces the elevated accumulation of *E. coli* near the gas interfaces compared to a wall, showing that the combined effects from interfacial hydrodynamics and Brownian dynamics play critical roles in determining cell accumulation near interfaces.

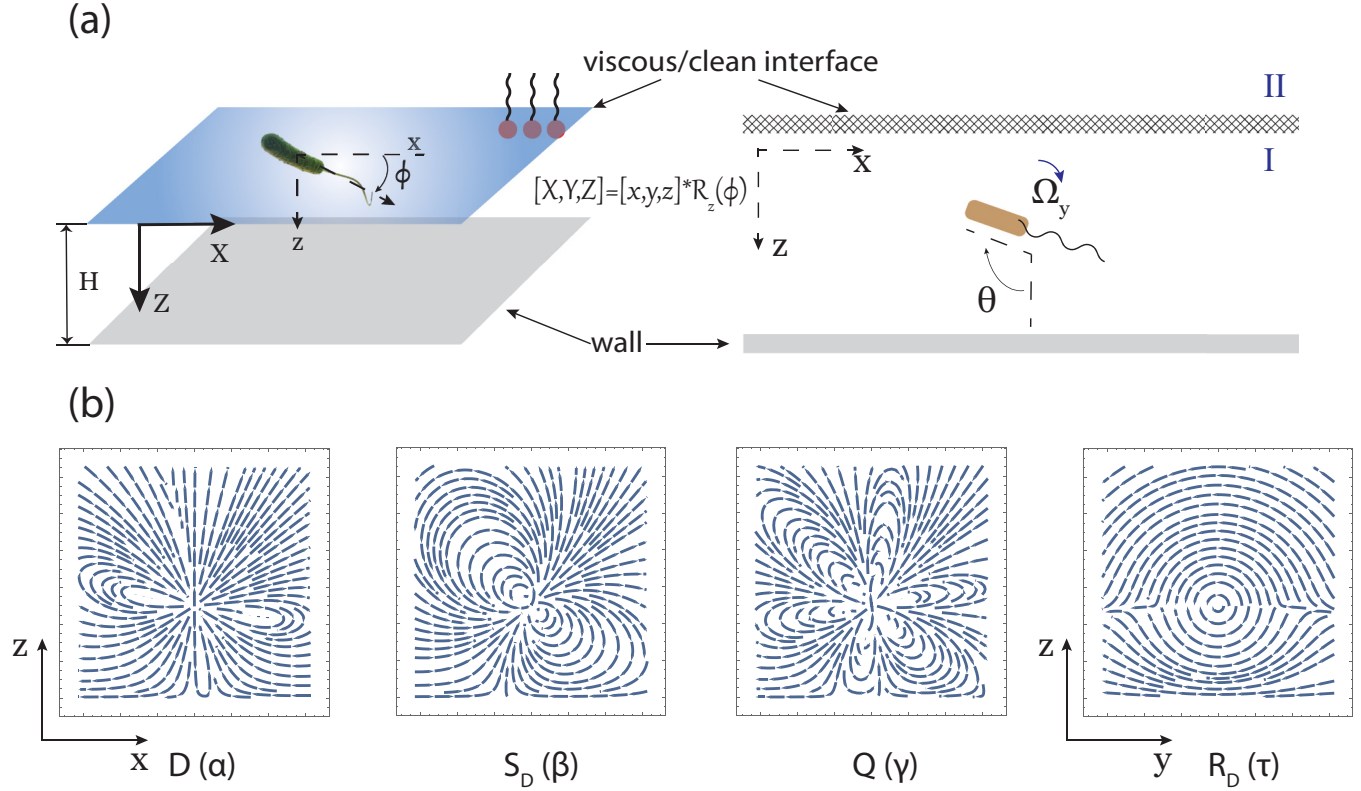


FIG. 3. (a) Schematic of bacteria swimming between a viscous interface and a solid wall in both global and local coordinates. (b) Flow fields generated by model bacteria near a clean CO_2 interface ($z = 0$): dipole (D), source doublet (S_D), quadrupole (Q), and rotlet dipole (R_D).

A. Modeling of flow around bacteria

The flow field around swimming bacteria is approximated as a linear combination of singularities [26],

$$\mathbf{u}_i = \alpha \mathbf{D} + \eta \mathbf{S}_D + \gamma \mathbf{Q} + \tau \mathbf{R}_D + O(|\mathbf{x} - \mathbf{x}_o|^{-4}), \quad (1)$$

where constants α , η , γ , and τ represent the strength of singularities. The force dipole D corresponds to the leading order flow field that is induced by the bacteria. In the next order, S_D is the source doublet, accounting for the finite size of bacteria, Q is the quadrupole singularity representing the length asymmetry between the appended flagella and the cell body, and rotlet dipole R_D accounts for the rotation of flagella and counterrotation of cell body [26].

By assuming the swimming direction $\mathbf{p} = (\sin \theta, 0, \cos \theta)$ in the x - z plane of the local coordinate [see Fig. 3(a)], the flow field generated by a force dipole (D) is

$$\mathbf{D}(\mathbf{x}, \mathbf{x}_o; \mathbf{p}) = \mathbf{p} \cdot \nabla_o \mathbf{G} = \left(\mathbf{p} \cdot \frac{\partial}{\partial \mathbf{x}_o} \right) \mathbf{G}, \quad (2)$$

$$\mathbf{G}(\mathbf{x}, \mathbf{x}_o; \mathbf{p}) = \frac{\mathbf{p}}{r} + \frac{(\mathbf{x} - \mathbf{x}_o)(\mathbf{x} - \mathbf{x}_o) \cdot \mathbf{p}}{r^3}, \quad (3)$$

where \mathbf{x}_o is the position vector of the swimmer, and $r = |\mathbf{x} - \mathbf{x}_o|$ is the magnitude of this position vector. Similarly, we express higher order singularities as $\mathbf{S}_D = -\nabla_o^2 \mathbf{G}/2$, $\mathbf{Q} = -(\mathbf{p} \cdot \nabla_o)^2 \mathbf{G}/2$, and $\mathbf{R}_D = -(\mathbf{p} \cdot \nabla_o) \nabla_o \times \mathbf{G}/2$. For flagellated bacteria such as *E. coli*, all coefficients are positive [27].

B. Surfactant-laden and clean interfaces

For a viscous interface such as surfactant-laden surface, our physical model includes tangential stress balance on the interface where Marangoni stress balances bulk viscous stress, and interfacial stress:

$$-\frac{\partial}{\partial x_i} \sigma - \mu_s \nabla_{\parallel}^2 u_i = \mu^I E_{iz}^I - \mu^{II} E_{iz}^{II}, \quad (4)$$

where μ_s is the interfacial shear viscosity, μ is the bulk viscosity, $\nabla_{\parallel}^2 = (\frac{\partial^2}{\partial x^2}, \frac{\partial^2}{\partial y^2}, 0)$, E_{ij} is the strain rate, and σ is the interfacial tension. (x, y, z) is the local coordinate attached to the bacterium in Fig. 3(a). The $z = 0$ plane, defined as the interface, separates two different fluid domains I and II, and a bacterium swims in domain I (bacteria solution, $z > 0$ region). For a surfactant-contaminated interface, σ can be nonuniform, leading to a Marangoni stress. We assume the interface to be incompressible [23]. From Eq. (4), three dimensionless parameters are

$$\beta = \frac{\mu_s}{\mu^I L}, \quad Ca = \frac{\mu^I U}{\sigma_o}, \quad \lambda = \frac{\mu^{II}}{\mu^I}, \quad (5)$$

where U is the swimming speed of bacteria, σ_o characterizes the interfacial tension of a clean interface, and L is the length of bacteria body plus flagella (typically, 1–2 μm for cell body and 7 μm for flagella bundles of *E. coli*), Ca is the capillary number, the ratio of the viscous force to the interfacial force, and β is the Boussinesq number, the ratio of interfacial viscosity to the fluid viscosity. *Escherichia coli* swimming in a bacteria solution with a mineral oil as

the top fluid ($\mu^I \sim 0.01 \text{ g cm}^{-1} \text{ s}^{-1}$, $U \sim 20 \mu\text{m s}^{-1}$, $\sigma_o \sim 28 \text{ mN/m}$) corresponds to Ca on the order of $O(10^{-7})$, and the associated interfacial deformation is negligible [28]. In our experiments, the interfacial viscosity is $\beta \sim 1\text{--}10^3$, where $\mu_s \sim 2.5 \times 10^{-7}\text{--}2.3 \times 10^{-5} \text{ N s/m}$, and the bulk viscosity is $\mu^I = 8.9 \times 10^{-4} \text{ N s/m}^2$ [29]. Therefore, the two significant parameters of the system are interfacial viscosity β and viscosity ratio λ . For clean interfaces, the variation of surface tension on the interface vanishes, where the bulk stresses of two fluids are equal at the interface. Equation (4) becomes $\mu^I E_{iz}^I = \mu^{II} E_{iz}^{II}$, and thus, the viscosity ratio λ solely determines the dynamics of clean interfaces.

For bacteria swimming near a liquid interface, the confinement induces extra flow, which is considered as the image flow \mathbf{u}^* . By treating the bacteria body as a spheroid with major axis $2a$ and minor axis $2b$, Faxén's law states that the induced translational and rotational velocities by the interface at the location of the bacterium are estimated as

$$\mathbf{U}^* = \mathbf{u}_o^* + O(a^2 \nabla^2 \mathbf{u}^*), \quad (6)$$

$$\boldsymbol{\Omega}^* = \frac{1}{2} \nabla \times \mathbf{u}_o^* + \chi \mathbf{p} \times (\mathbf{E} \cdot \mathbf{p})|_{x_o} + O[a^2 \nabla^2 (\nabla \times \mathbf{u}^*)], \quad (7)$$

where $\chi = \frac{a^2 - b^2}{a^2 + b^2}$ and $\mathbf{u}_o^* = \mathbf{u}^*|_{x_o}$.

C. Brownian dynamics simulations

We model bacteria dynamics by considering the hydrodynamic interactions between the interface and swimming bacteria, where there are negligible hydrodynamic interactions among bacteria due to their low volume concentrations.

The planar liquid interface alters the flow around the swimming bacteria [Fig. 3(b)]. To solve the flow field near the interface, we use the image singularity method to satisfy the interfacial stress condition Eq. (4) in the frequency domain using the Fourier transform. We have derived hydrodynamic effects of other higher order singularities on bacteria translation and rotation near the interface, where their derivation procedures are identical to the force dipole [23]. For simplicity, we show all results below. For the force dipole, the effect of interface on both translation and rotation are [$\mathbf{p} = (p_x, 0, p_z)$, and h is the distance between the swimming bacteria and the interface]

$$U_x^{\text{in},D} = \frac{3p_x p_z}{4h^2} - \frac{2p_x p_z}{\beta h} E_1, \quad (8)$$

$$U_z^{\text{in},D} = \frac{3(-1 + 3p_z^2)}{8h^2}, \quad (9)$$

$$\begin{aligned} \Omega_y^{\text{in},D} &= \frac{3p_x p_z}{16h^3} [2 + \chi(1 + p_z^2)] + p_x^2 \chi \left(\frac{p_x p_z}{\beta h^2} E_2 \right) \\ &+ p_x p_z \frac{2}{\beta h^2} [1 + \chi(p_z^2 - p_x^2)] E_2, \end{aligned} \quad (10)$$

where $l = \frac{\beta}{2(1+\lambda)}$ and

$$E_n = \frac{1}{2^n} \int_1^\infty \frac{\exp[(1-t)h/l]}{t^{n+1}} dt. \quad (11)$$

For source doublet, the effect of interface on both translation and rotation is simply the wall effect, and they are

$$U_x^{\text{in},S_D} = -\frac{p_x}{4h^3}, \quad (12)$$

$$U_z^{\text{in},S_D} = -\frac{p_z}{h^3}, \quad (13)$$

$$\Omega_y^{\text{in},S_D} = -3 \frac{p_x}{8h^4} \left[1 + \frac{3\chi}{2} (1 + p_z^2) \right]. \quad (14)$$

For quadrupole, they are

$$U_x^{\text{in},Q} = p_x \frac{1}{32h^3} (-7 + 27p_z^2) + \frac{p_x^3}{\beta h^2} (-E_2) + \frac{p_x p_z^2}{\beta h^2} (4E_2), \quad (15)$$

$$U_z^{\text{in},Q} = p_z \frac{1}{8h^3} (-7 + 9p_z^2), \quad (16)$$

$$\begin{aligned} \Omega_y^{\text{in},Q} &= \frac{3p_x (-1 + 3p_z^2)}{16h^5} + \chi \frac{3p_x}{64h^4} (-11 + 3p_z^4) \\ &+ p_x^3 [1 + \chi(p_z^2 - p_x^2)] \frac{3E_3}{2\beta h^3} \\ &+ 2p_x^2 p_z (-3\chi p_x p_z) \frac{E_3}{\beta h^3} \\ &+ p_x p_z^2 \frac{1}{\beta h^3} \left[-6E_3 - 12E_3 \frac{\chi}{2} (p_z^2 - p_x^2) \right]. \end{aligned} \quad (17)$$

Note that, for the rotlet dipole, we have

$$U_y^{\text{in},R_D} = \frac{p_x p_z}{\beta h^2} (-4E_2), \quad (18)$$

$$\begin{aligned} \Omega_x^{\text{in},R_D} &= \frac{3p_x p_z}{32h^4} [6 - \chi(1 + 3p_z^2)] + p_x^3 p_z \left(-\frac{3}{2\beta h^3} \chi E_3 \right) \\ &+ p_x p_z (-6 - 6\chi p_z^2) \frac{E_3}{\beta h^3}, \end{aligned} \quad (19)$$

$$\begin{aligned} \Omega_z^{\text{in},R_D} &= -\frac{3}{32h^4} [1 - 3p_z^2 - \chi p_x^2 (1 + 3p_z^2)] \\ &+ p_z^3 p_x (-6\chi E_3) \frac{1}{\beta h^3} + p_x^2 [3E_3 (1 + \chi/2)] \frac{1}{\beta h^3} \\ &+ p_x^2 p_z^2 (6\chi E_3) \frac{1}{\beta h^3}. \end{aligned} \quad (20)$$

To model the setup in Fig. 3(a), a recursive series of image systems are employed to include effects of both fluid interfaces and solid wall. Given the large distance $H = 500 \mu\text{m}$ between the liquid interface and the wall in the experiments, we estimate the boundary effect \mathbf{U}^{HI} by considering first two image systems, accounting for the hydrodynamic influence of interface and wall, respectively. Note that the effect of interface is including by an image singularity located at $z = -h$ while the effect of wall is due to the image singularity at $z = 2H - h$.

By considering interfacial hydrodynamics, swimming kinematics are modeled using stochastic differential equations,

$$\mathbf{U} = \mathbf{U}^{\text{sw}} + \mathbf{U}^{\text{HI}} + \mathbf{U}^{k_B T}, \quad (21)$$

$$\dot{\mathbf{p}} = (\boldsymbol{\Omega}^{\text{HI}} + \boldsymbol{\Omega}^{k_B T}) \times \mathbf{p}, \quad (22)$$

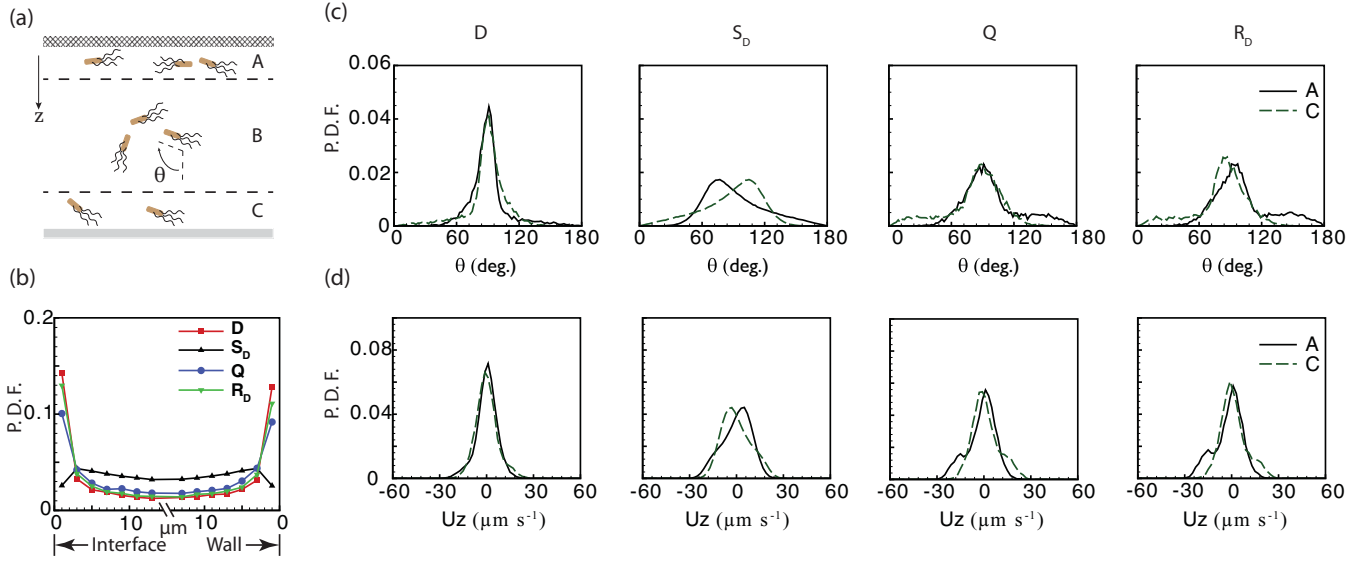


FIG. 4. (a) Schematic of bacteria swimming between viscous interface and solid wall along the vertical direction: near-interface region A, mid-region B, and near-wall region C. The probability density functions of (b) cells numbers, (c) bacteria orientation θ , and (d) vertical velocity U_z are calculated for various flow singularities in regions A and C: dipole (D , $\alpha = 21 \mu\text{m}^3 \text{s}^{-1}$), source doublet (S_D , $\eta = 21 \mu\text{m}^4 \text{s}^{-1}$), quadrupole (Q , $\gamma = 21 \mu\text{m}^4 \text{s}^{-1}$), and rotlet dipole (R_D , $\tau = 21 \mu\text{m}^4 \text{s}^{-1}$). The surface viscosity of the interface is given as $\beta = 1$, and viscosity ratio is $\lambda = 0.016$.

where $\mathbf{U}^{\text{sw}} = \mathbf{U} \cdot \mathbf{p}$ is the swimming speed of the bacteria, and $\dot{\mathbf{p}} = d\mathbf{p}/dt$. The interactions between interface or wall and bacteria are modeled as a short-range repulsive potential, accounting for the effects of van der Waals, electrostatic, and steric interactions [27,30]. Both $\mathbf{U}^{k_B T}$ and $\mathbf{\Omega}^{k_B T}$ describe stochastic dynamics due to thermal noise. In our simulations, the corresponding translational and rotational diffusivities are assumed to be isotropic and remain constant regardless of the bacteria position.

The computational domain is configured as $H \times H \times H$ where $H = 500 \mu\text{m}$. Periodic boundary conditions are used in both X and Y directions. In the Z direction, the top boundary ($Z = 0$) is set as interface, and the bottom boundary ($Z = H$) is the wall. To consider the effects of van der Waals, electrostatic, and steric interactions, we additionally impose short-range repulsion force whenever the bacterium is about to touch the interface or wall [27]:

$$U_z^{\text{SR}} = U \left[a^2 + (b^2 - a^2) p_x^2 \right]^6 \left[\frac{1}{h^{12}} - \frac{1}{(H-h)^{12}} \right], \quad (23)$$

$$\Omega_y^{\text{SR}} = 2p_x p_z \frac{a^2 |U_z^{\text{SR}}|}{\xi} \chi, \quad (24)$$

where $\xi = 5a$. The corresponding translational and rotational diffusivities are given as $0.18 \mu\text{m}^2/\text{s}$ and $0.05 \text{rad}^2/\text{s}$, respectively. Bacteria are initially randomly distributed within the simulation box with random orientation. Typically, bacteria distribution reaches steady state after 10 s.

D. Effect of individual singularities: Cell distribution, orientation, and translation

We examine how each flow singularity contributes to the distribution, orientation, and translation of cells near an interface and a solid wall. We divide the entire domain into three

regions along the vertical direction: the region near the interface [0–15 μm , denoted as “A” in Fig. 4(a)], the bulk region (15–485 μm , “B”), and the wall region (485–500 μm , “C”). In both regions A and C, force dipole (D), quadrupole (Q), and rotlet dipole (R_D) induce attraction to the interface and the solid wall, while source doublet (S_D) does not contribute to the accumulation near either boundary [Fig. 4(b)].

Both force dipole (D) and quadrupole (Q) induce a peak in the PDF of cell orientations θ at $\theta^p \sim 90^\circ$. Figure 4(c) shows that the force dipole leads to a more dominant peak in the horizontal orientation ($\theta^p \sim 90^\circ$) compared to quadrupole because of the leading order hydrodynamic effects. In addition, the probability of horizontal orientations $\theta^p = 90^\circ$ due to force dipole in region A (interface) is larger than that in region C (wall), which contributes to higher cell accumulation near the interfacial region.

Source doublet (S_D) and rotlet dipole (R_D) result in a peak in the PDF of cell orientations that is not exactly located in the horizontal direction [see Fig. 4(c)]. Our simulation results suggest that when the interfacial viscosity $\beta = 1$, the value of this deviation from the horizontal direction is about $|\theta^p - 90^\circ| \sim 5^\circ$ for the rotlet dipole, and $|\theta^p - 90^\circ| \sim 18^\circ$ for the source doublet. This finding explains the recent experimental discovery that cell bodies “nose down” near interfaces and walls, which exhibits a nonvanishing pitching angle near an air-liquid and liquid-solid surfaces (the time-averaged pitch angle (θ) $\sim 5^\circ$ in Ref. [15]).

Near a gas interface and a wall, the vertical swimming velocity peaks at $U_z^p \sim 0$ for force dipole (D), quadrupole (Q), and rotlet dipole (R_D) in Fig. 4(d). However, source doublet (S_D) induces nonzero vertical velocity, which reduces cell concentration near both interfaces and walls [Figs. 4(b) and 4(d)].

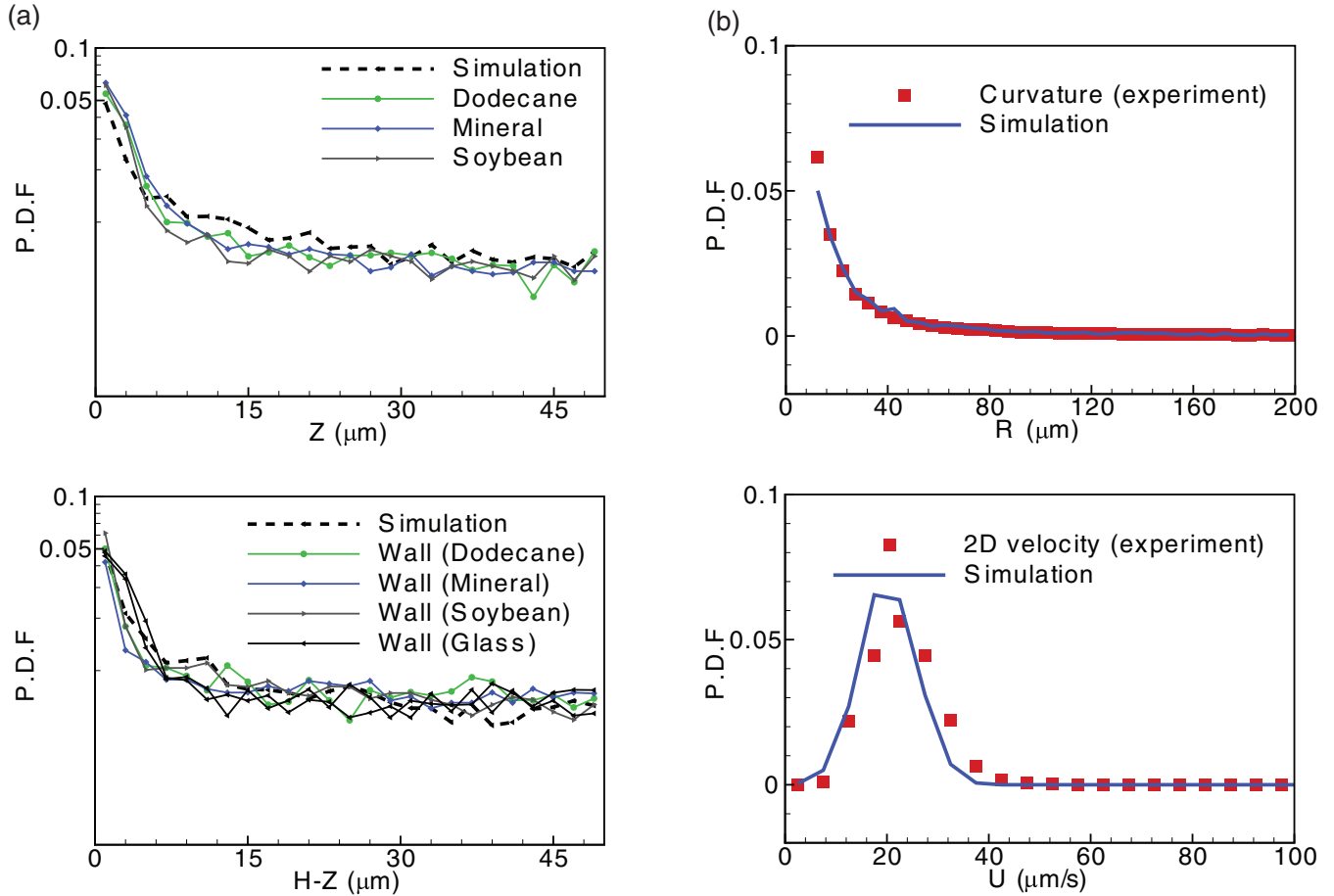


FIG. 5. (a) The comparison of probability density function between experimental (dodecane, mineral, soybean, and solid glasses) and numerical results. (b) The comparison of curvature and in-plane migration between experiments and simulation with the rotlet dipole (R_D) power of $\tau = 58 \mu\text{m}^4 \text{s}^{-1}$. The surface viscosity of the interface is $\beta = 1$.

IV. DISCUSSION

By converting the bacteria counts to the PDF, the results from experiments are compared to our model [Figs. 1(b) and 5(a)]. For the gas interface (i.e., CO_2) in Fig. 1(b), we observe higher accumulation near the interface than that from the wall, consistent with our model with $\beta = 1$. Therefore, both interfacial properties (e.g., interfacial viscosity) and Brownian dynamics contribute to the elevated cell concentration near the gas interface. However, for higher viscosity ratios such as dodecane, mineral, and soybean oils, the accumulation near interfaces is independent of viscosity ratios, which is close to the cases near the wall [see Fig. 5(a) and the Supplemental Material [21]]. Hence, there is a critical viscosity ratio, below which an elevated cell concentration occurs. In fact, in the following section on residence time, we show that this critical viscosity ratio is determined by interfacial viscosity β .

Our simulations show that there are equilibrium distributions of bacteria orientation in all regions, A, B, and C [see Fig. 1(c)]. The orientation distribution in both regions A and C near boundaries shows a higher probability of cell body direction to be close to horizontal $\theta \sim 90^\circ$ compared to that in region B, which explains the strong cell accumulation

near an interface or solid surface. Furthermore, similar to the previous experimental observation [15], our model shows that orientation distributions, in both regions A and C, do not peak exactly along the horizontal direction, which is due to higher order singularities.

A. Curvature and 2D velocity near liquid-solid surfaces

Besides the hydrodynamic trapping of cells close to the interfaces or wall, the literature has suggested that bacteria always undergo clockwise circular motion near the solid wall while there is a counterclockwise motion near a free interface [15,23]. For a clean liquid interface, the hydrodynamic analysis states that the flow singularity rotlet dipole (R_D) contributes to this in-plane circular motion, and the transition from clockwise to counterclockwise circular motion happens at the viscosity ratio $\lambda = (a/b)^2$: in the experiments, for *E. coli*, the aspect ratio of bacteria is around $a/b \sim 5$, and therefore, the transition should happen at a viscosity ratio of $\lambda \sim 25$ near clean interfaces. However, we observe the clockwise motion in the population of cells near CO_2 and dodecane liquid interfaces in the experiments, which occurs due to the hydrodynamic effects of interfacial viscosity [see Fig. 6(a)]. In the experiments, we track bacteria trajectories near the wall

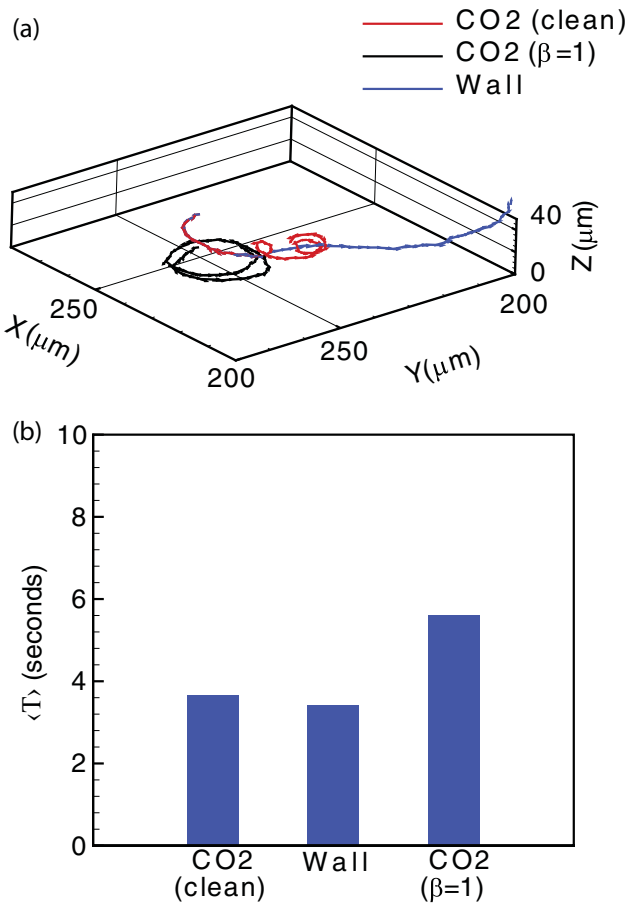


FIG. 6. (a) Showcase of bacteria trajectories simulated near different surfaces. (b) Ensemble average of residence time over 10^3 realizations. The time duration is 6 s with force dipole (D) of $\alpha = 34 \mu\text{m}^3 \text{s}^{-1}$ and rotlet dipole (R_D) of $\tau = 58 \mu\text{m}^4 \text{s}^{-1}$.

and determine the distribution of local curvature of trajectories and swimming speed, which is well predicted with our model using the power of rotlet dipole (R_D) illustrated in Fig. 5(b).

B. Role of hydrodynamic effects on residence time

Next, we examine the residence time of bacteria near the clean or surfactant-contaminated interfaces and solid surfaces. In Fig. 6(b) the time duration of bacteria near the clean interface is close to that near the wall, whereas bacteria reside longest near the surfactant-contaminated interface. The bacteria residence time near interfaces or surfaces is due to the hydrodynamic reorientation of bacteria: faster reorientation towards the interface prevents cells from escaping the interfaces and wall. The balance between hydrodynamic attraction and cell rotational diffusion, as stated in Eq. (22), governs the residence time of bacteria near different interfaces [Fig. 6(a)].

The hydrodynamic effects on the rotation of bacteria depend on the value of interfacial viscosity (see Fig. S2 in the Supplemental Material [21]). The rate of bacteria rotation near the interface is larger than the one near the solid wall ($\beta \sim 1$), and the magnitude of Ω^{HI} is the largest when there is a CO₂ interface (lowest viscosity ratio in our experiments). This explains our experimental finding of high cell accumulation near CO₂ interface shown in Fig. 1(b).

When the viscosity ratio λ is large, the rotation rate of bacteria near interfaces is closer to that near a wall. For $\beta = 1$, our simulations suggest that cell densities near liquid interfaces are similar to that near the wall when viscosity ratio $\lambda > 1$. Therefore, the cell density near liquid interfaces is independent of viscosity ratio, which explains our experimental findings on cell accumulations with dodecane, mineral, and soybean oils [Fig. 5(a)].

Under large values of interfacial viscosity $\beta \sim O(10^3)$, the rate of rotation is always independent of viscosity ratio, and accumulations near both gas and liquid interfaces are close to the case of a solid wall (see Fig. S2 in the Supplemental Material [21]).

V. CONCLUSIONS

We have presented vertical distributions of bacteria in the vicinity of fluid interfaces via combined numerical, theoretical, and experimental analyses. By incorporating interfacial hydrodynamics, we developed a model to explain bacteria dynamics in a confined domain, such as cell accumulation and inclination of cell bodies from the horizontal direction near an interface or wall. Given the small size of bacteria leading to negligible capillary effects, we show that both interfacial viscosity and viscosity ratio of two fluids play important roles in determining the cell distribution when interfacial viscosity is small (e.g., an amphiphilic bilayer). However, this distribution is independent of the viscosity ratio when the interfacial viscosity is large.

Data are publicly available through the Gulf of Mexico Research Initiative Information & Data Cooperative (GRIIDC) at Ref. [31].

ACKNOWLEDGMENTS

We thank N. Desai for a discussion on the determination of rotlet dipole power. We also thank A. J. T. M. Mathijssen for the discussion of bacteria “nose down” behavior near interfaces. This work is partially supported by grants from the Gulf of Mexico Research Initiative and the National Science Foundation CBET-1604423 and CBET-1700961. This work used the Extreme Science and Engineering Discovery Environment (XSEDE), which is supported by National Science Foundation Grants No. CTS190041 and No. CTS190055.

A.A. and S.W. equally contributed to this work.

- [1] K. Drescher, Y. Shen, B. L. Bassler, and H. A. Stone, *Proc. Natl. Acad. Sci. USA* **110**, 4345 (2013).
 [2] S. Das, A. Garg, A. I. Campbell, J. Howse, A. Sen, D. Velegol, R. Golestanian, and S. J. Ebbens, *Nat. Commun.* **6**, 8999 (2015).

- [3] L. J. Fauci and A. McDonald, *Bull. Math. Biol.* **57**, 679 (1995).
 [4] K. A. Prather, T. H. Bertram, V. H. Grassian, G. B. Deane, M. D. Stokes, P. J. DeMott, L. I. Aluwihare, B. P. Palenik,

- F. Azam, J. H. Seinfeld *et al.*, *Proc. Natl. Acad. Sci. USA* **110**, 7550 (2013).
- [5] A. P. Berke, L. Turner, H. C. Berg, and E. Lauga, *Phys. Rev. Lett.* **101**, 038102 (2008).
- [6] M. Molaie, M. Barry, R. Stocker, and J. Sheng, *Phys. Rev. Lett.* **113**, 068103 (2014).
- [7] H. Jashnsaz, M. Al Juboori, C. Weistuch, N. Miller, T. Nguyen, V. Meyerhoff, B. McCoy, S. Perkins, R. Wallgren, B. D. Ray *et al.*, *Biophys. J.* **112**, 1282 (2017).
- [8] Rothschild, *Nature (London)* **198**, 1221 (1963).
- [9] E. A. Dubinsky, M. E. Conrad, R. Chakraborty, M. Bill, S. E. Borglin, J. T. Hollibaugh, O. U. Mason, Y. M. Piceno, F. C. Reid, W. T. Stringfellow *et al.*, *Environ. Sci. Technol.* **47**, 10860 (2013).
- [10] L. Friedman and R. Kolter, *J. Bacteriol.* **186**, 4457 (2004).
- [11] L. Vaccari, M. Molaie, T. H. Niepa, D. Lee, R. L. Leheny, and K. J. Stebe, *Adv. Colloid Interface Sci.* **247**, 561 (2017).
- [12] C. Wu, J. Y. Lim, G. G. Fuller, and L. Cegelski, *Biophys. J.* **103**, 464 (2012).
- [13] B. A. Grzybowski, H. A. Stone, and G. M. Whitesides, *Nature (London)* **405**, 1033 (2000).
- [14] D. M. Kaz, R. McGorty, M. Mani, M. P. Brenner, and V. N. Manoharan, *Nat. Mater.* **11**, 138 (2012).
- [15] S. Bianchi, F. Saglimbeni, G. Frangipane, D. Dell'Arciprete, and R. Di Leonardo, *Soft Matter* **15**, 3397 (2019).
- [16] G. Li, L.-K. Tam, and J. X. Tang, *Proc. Natl. Acad. Sci. USA* **105**, 18355 (2008).
- [17] A. Be'er and R. M. Harshey, *Biophys. J.* **101**, 1017 (2011).
- [18] S. Bianchi, F. Saglimbeni, and R. Di Leonardo, *Phys. Rev. X* **7**, 011010 (2017).
- [19] N. D. Cardwell, P. P. Vlachos, and K. A. Thole, *Meas. Sci. Technol.* **22**, 105406 (2011).
- [20] T. Guo, A. M. Ardekani, and P. P. Vlachos, *Exp. Fluids* **60**, 89 (2019).
- [21] See Supplemental Material at <http://link.aps.org/supplemental/10.1103/PhysRevE.100.062605> for a summary of box plots for all viscosity ratio in Sec. s1. Section s2 describes rotational velocity as a function of bacteria orientation for both surfactant-contaminated and clean interfaces .
- [22] G. Li and J. X. Tang, *Phys. Rev. Lett.* **103**, 078101 (2009).
- [23] D. Lopez and E. Lauga, *Phys. Fluids* **26**, 071902 (2014).
- [24] N. Desai, V. A. Shaik, and A. M. Ardekani, *Soft Matter* **14**, 264 (2018).
- [25] M. Morse, A. Huang, G. Li, M. R. Maxey, and J. X. Tang, *Biophys. J.* **105**, 21 (2013).
- [26] S. E. Spagnolie and E. Lauga, *J. Fluid Mech.* **700**, 105 (2012).
- [27] A. J. Mathijssen, A. Doostmohammadi, J. M. Yeomans, and T. N. Shendruk, *J. Fluid Mech.* **806**, 35 (2016).
- [28] S. Wang and A. M. Ardekani, *Phys. Rev. E* **87**, 063010 (2013).
- [29] L. Vaccari, D. B. Allan, N. Sharifi-Mood, A. R. Singh, R. L. Leheny, and K. J. Stebe, *Soft Matter* **11**, 6062 (2015).
- [30] J. Hu, A. Wysocki, R. G. Winkler, and G. Gompper, *Sci. Rep.* **5**, 9586 (2015).
- [31] <https://data.gulfresearchinitiative.org>, doi: 10.7266/WGAQQWN8.